Coherent ultrafast lattice-directed reaction dynamics of triiodide anion photodissociation

Coherent ultrafast lattice-directed reaction dynamics of triiodide anion photodissociation

Rui Xian[1,5], Gastón Corthey[1], David M. Rogers[2], Carole A. Morrison[2], Valentyn I. Prokhorenko[1], Stuart A. Hayes[1], and R. J. Dwayne Miller[*1,3,4]

[1] Max Planck Institute for the Structure and Dynamics of Matter, Luruper Chaussee 149, 22761 Hamburg, Germany

[2] School of Chemistry and EaStCHEM Research School, University of Edinburgh, The King's Buildings, David Brewster Road, Edinburgh EH9 3FJ, United Kingdom

[3] Departments of Chemistry and Physics, University of Toronto, 80 St. George Street, Toronto M5S 3H6, Canada

[4] Hamburg Center for Ultrafast Imaging, Luruper Chaussee 149, 22761 Hamburg, Germany

[5] Present address: Fritz-Haber-Institut der Max-Planck-Gesellschaft, Faradayweg 4-6, Berlin 14195, Germany

* dwayne.miller@mpsd.mpg.de

Solid-state reactions are influenced by the spatial arrangement of the reactants and the electrostatic environment of the lattice, which may enable lattice-directed chemical dynamics. Unlike the caging imposed by an inert matrix, an active lattice participates in the reaction, however, little evidence of such lattice participation has been gathered on ultrafast timescales due to the irreversibility of solid-state chemical systems. Here, by lowering the temperature to 80 K, we have been able to study the dissociative photochemistry of the triiodide anion (I_3^-) in single-crystal tetra-*n*-butylammonium triiodide using broadband transient absorption spectroscopy. We identified the coherently formed tetraiodide radical anion ($I_4^{-\bullet}$) as a reaction intermediate. Its delayed appearance after that of the primary photoproduct, diiodide radical ($I_2^{-\bullet}$) indicates that $I_4^{-\bullet}$ was formed via a secondary reaction between a dissociated iodine radical ($I^\bullet$) and an adjacent I_3^-. This chemistry occurs as a result of the intermolecular interaction determined by the crystalline arrangement and is in stark contrast with previous solution studies.

System-bath interaction (SBI) is the distinguishing feature of condensed-phase chemistry[1]. In this context, the reactants constitute the system of interest and the molecular environment (i.e. solvent or lattice) functions as the bath. The system

and the bath are coupled via intermolecular interactions of various origins, which exert influence in the chemical dynamics unfolding on different timescales. While the interaction between the solute and the solvent-bath has attracted great attention for ultrafast studies[2–5], the influence of the crystal lattice has been mostly investigated in doped inert matrices[6] but little explored in bulk single crystals, in which the reactants form part of the lattice. In the latter case, chemical dynamics initiated by external stimuli can induce cascaded reactions promoted by SBI as a result of the spatial arrangement of the reactants within the lattice. Here we use a model photochemical system, the triiodide anion (I_3^-), to illustrate this. As one of the best-studied molecular systems, I_3^- possesses only three or four vibrational degrees of freedom in its bent or linear geometries, which provides a much better defined probe for SBI than the more complex systems. Even within this relatively small system, there is a wealth of interactions that probe nearly all aspects of the SBI. The I_3^- anion dissociates into various iodine-containing fragments[7,8] upon photoexcitation to either of its two major absorption bands (labelled C and D in Fig. 1b). The conical-intersection-mediated[8] bond-breaking event takes place within a few hundred femtoseconds after photoexcitation, allowing the transfer of vibrational coherence from the reactant to the principal diatomic photoproduct, diiodide radical ($I_2^{-\bullet}$), in condensed phases[9–12]. The strength of the SBI is quantifiable by the vibrational dephasing time of $I_2^{-\bullet}$,[11] the recombination rate of $I_2^{-\bullet}$,[13] and the recovery rate of the ground-state I_3^-.[14]

To investigate the influence of SBI on I_3^- photodissociation in solid-state systems requires tackling the irreversibility of the reaction. To date, the only published ultrafast study on solid-state triiodide[13] employed spatially-encoded single-shot spectroscopy. The speed-up of the recombination in crystals with stricter spatial confinement of the reactant was direct evidence of lattice caging. However, the single-shot method applied in that study was limited to single-wavelength probing from the dual-echelon design, and suffered from low signal-to-noise ratio (SNR) due to low probe transmission through thick sample[11]. The limited photocycles of the sample at room temperature has placed stringent constraints on the time-delay range that can be measured on a single sample. To improve the measurement conditions, we studied the reaction in ultramicrotomed thin crystalline samples at 80 K by measuring the transient absorption (TA) following 400 nm photoexcitation with a supercontinuum probe covering both the triiodide and the diiodide bands. We chose to study tetra-*n*-butylammonium triiodide (*n*-Bu_4NI_3, or TBAT) since the I_3^- chains are strictly confined in the 1D channels (see Fig. 1a) laid out by the counterion framework, implying a strong SBI. We first demonstrate this computationally by comparing gas-phase and solid-state quantum chemical calculations of the electronic structure of I_3^-, which can explain the spectroscopic signatures produced by the lattice influence from that of isolated I_3^-. Then, in our TA experiment, through a combination of global analysis, time-frequency analysis and Fourier-filtering, we found clear evidence of coherent $I_4^{-\bullet}$ formation via a secondary reaction that takes place within a few ps of photoexcitation, and concurrent lattice perturbations conducive to the reaction. These two aspects of lattice participation complement the known influence of the SBI (i.e. lattice caging) pertaining to this model photochemical reaction in single crystals.

Results and discussion

Consequences of the crystalline environment on the system-bath coupling. The I_3^- chains exhibit high structural malleability in solution[15,16] and in the solid state[17] as a result of electrostatic interactions with their surroundings. The solid-state absorption spectrum of TBAT is remarkably more complex than that in ethanol solution (see Fig. 1b). While the solvated I_3^- spectrum is dominated by the C, D and E bands in the UV-NIR region, the solid-state TBAT spectrum displays much more intense A and B bands (both are spin-flip transitions), spectral broadening in all bands, as well as band-specific polarization dependence. This significant difference in the absorption spectra is mainly due to the existence of two types of I_3^- chains (named straight and bent chains) in TBAT due to intermolecular interactions (IMI), and are identifiable in the resonance Raman spectrum.[18,19] This manifestation of IMI has been termed the Craig effect in the context of organic molecular crystals exhibiting configurational mixing of electronic states.[20] These two types of I_3^- chains represent the two independent anions in the asymmetric unit of the TBAT unit cell. In effect, each type of I_3^- chain produces a set of bands and most of them are well separated by tens of nanometers in the spectra due to differences in the molecular orbital (MO) energies (see Fig. 1d-g).

Physically, the differences in MO energies can be associated with a DC Stark effect caused by the permanent electric dipole moment a bent I_3^- chain possesses in relation to the ionic lattice, which is absent in its linear optimized gas-phase structure. Density of states (DoS) calculations in solid state (see Fig. 1f-g) show significant changes in the electronic structure from gas phase due to IMI, which causes further broadening of the absorption bands that give rise to the observed spectra. The calculations for solid-state TBAT also revealed that electronic transitions in the UV-NIR energy range are localized to I_3^-, therefore, the 400 nm photoexcitation targets only the triiodide part of the unit cell. The counterions do provide the structural scaffolding that orients the I_3^- along the **a** axis, thereby limiting their motion. This provides a necessary condition for lattice-directed reaction dynamics.

Transient absorption measurements. We measured the low-temperature transient absorption of the sample using the experimental setup described in the Methods section. At 80 K, coherent dynamics persist beyond 10 ps after photoexcitation (see Fig. 2a). A continuation of fast oscillations with frequencies similar to the stretching modes of I_3^- and $I_2^{-\bullet}$ is visible up to a probe delay of ~ 6 ps across most of the probe spectrum, although the instability of the supercontinuum probe near the pump wavelength (800 nm) washed out the coherent dynamics in neighboring spectral regions.

The sign of the TA signal presents an obvious choice for dividing the probe spectrum into the reactant- and the photoproduct-dominating bands, despite the overlapping absorption bands of the different chemical species involved in the

reaction (see Fig. 1b-c). The location of a major $I_2^{-\bullet}$ absorption band (X → A′) in the 700-800 nm region is in good agreement with previous condensed-phase studies[10,11,24]. Further justification is found from the 2D power spectrum (see Fig. 2b) of the global-analysis[25] residuals, calculated using Welch's frequency estimation method[26] (see Supplementary Information, Section 3.1). The downward frequency shift in the 100-125 cm^{-1} region from the short to the long wavelength side of the probe spectrum in Fig. 2b is a clear manifestation of the gradual change of molecular character, since the symmetric stretching mode of I_3^- (110-112 cm^{-1}) has slightly higher frequency than the stretching mode of $I_2^{-\bullet}$ (e.g. 102-106 cm^{-1}), as established in previous solution-phase studies[9,12,22] and in our DFT calculations (see Supplementary Table 2-3).

To visualize the time evolution of the frequency components, we applied continuous wavelet transform (CWT)[27] to the time-series data. The panels in Fig. 2c-e show the results from CWT of the residuals at three probe wavelengths (461 nm, 606 nm and 713 nm) that characterize distinct regions of the TA spectra (Fig. 2a). The major frequencies retrieved from the analysis are tabulated in Supplementary Table 1, along with available assignments.

Interpretation of the reaction intermediates and pathways. Transient absorption spectra contain information on electronic population dynamics and coherent nuclear signatures, which can be exploited to identify reaction intermediates and infer reaction pathways. To unravel the complexity in the overlapping absorption spectra, we Fourier-filtered[28] the global analysis residuals at each wavelength to single out frequency components of interest (see Fig. 3a-b). The filtering markedly improved the visibility of the π phase jumps of the oscillations that were buried in the residuals (see Supplementary Fig. 12), The node (i.e. zero-crossing) of the phase jump can be used as a marker of absorption peak[9,28–30] in femtosecond TA measurements involving impulsively excited modes, since wavepacket motion of the hot ground-state photoproduct around its energy minimum manifests itself in the antiphase oscillations observed at wavelengths about equally distant on opposite sides of the absorption maximum. For coherently formed ground-state $I_2^{-\bullet}$, its low-lying X → A′ absorption band contributes a node at its peak around 750 nm, as shown in previous solution[9,10] and solid-state[11] TA experiments. Filtered at center frequencies of 22 cm^{-1} and 33 cm^{-1} (see Fig. 3a-b), the residuals show a node at ~ 482 nm for both frequencies, and an additional node at ~ 587 nm, but only for the 33 cm^{-1} mode. Since 22 cm^{-1} is a libration mode of I_3^- in TBAT[19], the 482 nm node can be assigned to the ground-state I_3^- (possibly the B band, see Fig. 1b), but the 587 nm node points to another coherently evolving molecular species involved in the reaction. From the known absorption spectra of polyiodides[31], a very close match is found in $I_4^{-\bullet}$ (see Fig. 1c). Therefore, the delayed appearance of the 33 cm^{-1} mode is better associated with the emergence of $I_4^{-\bullet}$ given its high temporal correlation with the growing signature at a probe delay of 2-6 ps in Fig. 2d and 3c. The appearance and decay of this positive signal in the TA spectra at 590-640 nm (see Fig. 3d-e) and its gradual separation from the X → A′ band of $I_2^{-\bullet}$ further supports the assignment to $I_4^{-\bullet}$.

On the other hand, the timescales and spectral information contained in the DAS also lend support to $I_4^{-\bullet}$ formation. The six DAS within a probe delay of 1 ns are shown in Fig. 3f. The first one, with a lifetime of 65 fs, was regarded as coherent cross-phase modulation or fast electronic processes that cannot be fully resolved with the time resolution of our experimental setup (FWHM of the wavelength-dependent instrument response function is ~ 100-150 fs). The other five represent different stages of the chemical dynamics.

Kinetic evidence from a previous flash photolysis study[23] showed that $I_4^{-\bullet}$ can be formed from bonding of the highly reactive $I^\bullet$ to I_3^-. In that study, the former intermediate came from the photodissociation of I_2, while the latter was present in the solution as a result of the chemical equilibrium between I_2 and I^-. In our study, a similar situation exists, but here, $I^\bullet$ is provided by the photodissociation of I_3^- through a two-body photodissociation channel, and the I_3^- very likely comes from a neighboring lattice site that was lying right along the dissociation trajectory of $I^\bullet$. The well-aligned I_3^- chains in the TBAT crystal and the high polarizability of inter-iodine bonds increase the chance of long-chain formation. Hence, we postulate that the production of $I_4^{-\bullet}$ in crystalline TBAT can be described by the following two-step reaction,

$$I_3^- \xrightarrow{h\nu} I_2^{-\bullet} + I^\bullet \qquad \text{(a)}$$

$$I^\bullet + I_3^- \rightleftharpoons I_4^{-\bullet} \qquad \text{(b)}$$

The negative and positive features in DAS signal growth and decay of electronic population, respectively. With help from the available absorption spectra of related species (see Fig. 1b-c), we can relate the signatures in the region > 650 nm and around 587 nm to $I_2^{-\bullet}$ and $I_4^{-\bullet}$, respectively. The timescales of the remaining five DAS (see Fig. 3f) can be interpreted as: (2) $I_2^{-\bullet}$ formation; (3) first phase of $I_2^{-\bullet}$ recombination and onset of $I_4^{-\bullet}$ formation from $I^\bullet$ and I_3^-; (4) start of $I_4^{-\bullet}$ dissociation reaction; (5)-(6) I_3^- recovery and $I_2^{-\bullet}$ recombination. The two-step reaction scheme requires a separation of timescales of $I_2^{-\bullet}$ and $I_4^{-\bullet}$ formation. The evidence of this time lag is emphasized in Fig. 3e between the probe delay of 0-5 ps in the $I_2^{-\bullet}$ and $I_4^{-\bullet}$ bands. Furthermore, matrix-isolation spectroscopy[32] and quantum chemical calculations (see Supplementary Table 8) provided support that $I_4^{-\bullet}$ possesses electronic transitions below 500 nm, which can explain the bands appearing between 490 nm and 520 nm, as well as in the region < 450 nm in DAS (3)-(4). Both of these two bands emerge and decay in sync with the 587 nm band of $I_4^{-\bullet}$ in the DAS, and therefore should have the same association. The positive signatures of the $I_2^{-\bullet}$ and $I_4^{-\bullet}$ formation and the negative signature of the ground-state bleaching of I_3^- contribute to the complexity seen in the DAS, e.g. the dispersive profile of DAS (3)-(4) around 587 nm.

Finally, we fitted the global analysis residuals to extract the lifetimes of the oscillatory features at different probe wavelengths following Ref. 33, The results summarized in Section 3.2 of the Supplementary Information show that while most of the coherent oscillations have lifetimes on the order of 0.5-3 ps, the I_3^- lattice modes of 13 cm^{-1} and 31 cm^{-1} decay on 6-10 ps, which goes beyond the timescale of $I_4^{-\bullet}$ formation (see Fig. 2d). This indicates that the lattice dynamics is still coherent when the secondary reaction takes place, giving rise to coherently formed $I_4^{-\bullet}$. Both of these modes are of

librational or translational characters, which can couple $I^{\bullet}$ and I_3^- directly into the product state. In addition, the lattice modes also provide dissipation channels to accommodate the excess energy released in the reaction.

The evidence of the appearance of $I_4^{-\bullet}$ as a reaction intermediate has brought to the forefront the possibility of bond formation due to selective intermolecular interaction in the solid state on ultrafast timescales. In our study, this scenario is more plausible for light species like $I^{\bullet}$ than its diatomic co-product $I_2^{-\bullet}$ with an adjacent I_3^-, because the excess translation energy imparted to $I_2^{-\bullet}$ from bond-breaking will, according to momentum conservation, grant it only half of the recoil velocity as $I^{\bullet}$, and it will be further slowed down by the Coulombic repulsion from I_3^-. The alternative two-body dissociation channel ($I_3^- \xrightarrow{h\nu} I_2 + I^-$) contains a distinct monatomic fragment, the iodide anion (I^-), but its reactivity is low and the formation of the dianion I_4^{2-} through an analogous bimolecular association pathway, $I^- + I_3^- \rightleftharpoons I_4^{2-}$, is thermodynamically discouraged[34,35]. Furthermore, the other photofragment, I_2, will generate the well-characterized absorptive signal in the region of 500-600 nm from its major absorption bands[36], and will follow different kinetics with respect to the spectral region dominated by $I_2^{-\bullet}$ formation. However, these I_2 signatures have not been observed in our experiments. The low TA signal in the spectral region of 550-590 nm from all time delays contrasts starkly with the emergence of the $I_2^{-\bullet}$ band in the near-IR region (see Fig. 2a and 3d), this supports an explanation invoking only $I_2^{-\bullet}$ and $I_4^{-\bullet}$. A possible reaction mechanism derived from our analysis is sketched in Fig. 4.

Comparison with solution-phase results. I_3^- undergoes dissociation from its C band in both solution and solid state. The dividing line, however, lies in the secondary reactions starting with spatially separated photofragments. The reactive encounters between $I^{\bullet}$ and I_3^- should be present after I_3^- photodissociation in solution, but they are outrun by competing secondary processes such as the geminate recombination of $I^{\bullet}$ and $I_2^{-\bullet}$ within the same solvent shell. The bimolecular $I_4^{-\bullet}$ formation reaction does not contribute significantly to the measured TA signal. In solid-state TBAT, however, the dissociated $I^{\bullet}$ fragment proceeds in a very restricted pathway determined by the geometry of the space in which the reactants reside. Therefore, $I_4^{-\bullet}$ formation becomes a dominant process and is well observable in TA measurements. To our knowledge, $I_4^{-\bullet}$ formation as a secondary reaction pathway has not been observed in previous femtosecond TA studies on I_3^- in condensed phases[9–12,14,22,38]. The use of thin single-crystal samples, broadband probe and significantly improved SNR allowed us to capture these reaction details.

The observations made in the present study allow us to compare solution and solid-state TA experiments in a general sense. In solution phase, solvent friction results in rapid vibrational decoherence of solute molecules, therefore typically only fast coherent modes with periods not much longer than the mean free time between collisions (on the order of a few hundreds of fs)[39] can survive dephasing. They appear as underdamped oscillations modulating the electronic TA spectra in the UV-NIR range[40], or as population dynamics in electronic-vibrational TA spectra in the mid-IR range[41]. The collective

modes of the solvent bath are usually overdamped and therefore not spectroscopically discernible. In molecular crystals, however, the bath modes are well-defined (external) lattice modes and are greatly enhanced by the translational symmetry of the crystal. The internal (molecular) modes are coupled to the lattice modes and yet still retain their molecular characters[42], therefore, molecular motions initiated by chemical reactions are directly translated into lattice excitation. In addition, the limited mobility of the molecular species in the crystal slows down decoherence, which allows the slow bath modes to be captured via optical means. In this sense, solid-state experiments has the distinct advantage in that information on the coherent and population dynamics do not suffer from averaging of isotropic ensembles, as is the case of solution-phase studies. New information on the directional aspects of the chemistry is revealed as the present case has shown.

Conclusion

We investigated the molecular and lattice dynamics following the photodissociation of I_3^- in the solid state (TBAT single crystals) from 400 nm photoexcitation to its C band. Using broadband probe, global analysis and advanced frequency analysis, along with structural and electronic information obtained from theoretical calculations, we unraveled the complexity of the problem and isolated distinctive spectroscopic features of the $I_4^{-\bullet}$ intermediate. We proposed a reaction scheme taking into account the intermolecular interactions between well-aligned adjacent I_3^- chains in the highly reactive ionic environment to explain our observation. Moreover, we identified prominent coherent lattice perturbations linked to $I_4^{-\bullet}$ formation. These aspects constitute coherent and ultrafast lattice accommodation of reactive species and provide experimental evidence that lattice-coupled reactive systems exhibit stereochemical selection determined by the local bath geometry, in addition to the caging effect an inert bath (e.g. inert solvent or solid matrix) imposes. Our results suggest that the corresponding gas-phase reaction scheme needs to be significantly modified to take full account of the system-bath interactions in the crystalline environment (between reactant, photoproduct and lattice). The very recent surge of interest[43–45] in the study of the coupling of lattice dynamics to various reactive molecular systems on ultrafast timescales also demonstrate the varieties of lattice participation, which will require investigation on a case-by-case basis to eventually arrive at a generalized description of lattice-coupled reaction dynamics. Furthermore, our study motivates future work to verify the present findings using structure-resolving probes[46] that directly access the spatial degrees of freedom, which are fundamental to understanding chemistry.

Methods

Sample preparation. Commercially available tetra-*n*-butylammonium triiodide (Sigma-Aldrich, ≥ 97.0%) was used for crystallization using the solvent evaporation method from ethanol solution. The crystals were wet-cut on water using an ultramicrotome (Leica EM UC7)

close to their long axes (crystallographic **a** axis) to produce samples with a thickness of ~ 1 μm (OD ~ 1 at 400 nm). The cut slices were harvested and dried on fused silica substrates before optical measurements.

Optical measurements. The steady-state absorption spectra of solid-state TBAT were measured with a home-built microspectrometer[47] employing a fiber-coupled deuterium halogen lamp (Ocean Optics, DH-2000-BAL) with ~ 100 μm focus size at the sample position. The solution spectra were measured with quartz cuvettes in a commercial spectrophotometer (Shimadzu UV-2600). The low-temperature transient absorption measurements were performed in a liquid nitrogen cryostat (Oxford Instruments, Optistat DN-V2). Both pump and probe pulses were derived from the same ultrafast Ti:Sapphire laser (Coherent Legend Elite USP) with 40 fs, 800 nm outputs operating at 500 Hz. To accommodate the slow recovery rate of the sample, a chopper was used to reduce the overall repetition rate to 250 Hz. The 400 nm pulses from the second harmonic generation of 800 nm laser fundamental ran at 125 Hz during the measurements with an excitation fluence of 0.29 mJ/cm^2 (5.8 × 10^{14} photons/cm^2). The probe was 800 nm-pumped supercontinuum generated in ultrapure water. The 800 nm residual in the supercontinuum was filtered out before the sample. The transmitted probe was detected at every shot using a home-built spectrometer with fast electronics. Further details are provided in Supplementary Information, Section 1.3.

Computation. The crystal structure[21] of TBAT obtained from the Cambridge Structural Database (CSD) was optimized using the PBE[48] density functional and Tkatchenko and Scheffler dispersion correction scheme[49] in CASTEP 8.0. Norm-conserving 'recpot' pseudopotentials were used for each element. The optimization of atomic positions and unit cell vectors were carried out simultaneously using the BFGS method within the symmetry constraints of the unit cell ($P\bar{1}$ symmetry). The resulting structure was then used to compute electronic band structure (Supplementary Fig. 13), density of states (Fig. 1f), and partial density of states (Fig. 1g). Density functional theory (DFT) calculations of the normal modes of iodine species (I_2, I_n^- with n = 2, 3, 4) also employed the PBE pure exchange and correlation functional. They were carried out for optimized geometries in the gas phase and in a polarizable continuum model (PCM) with *n*-pentane as the solvent to simulate the environment effect. The symmetry is D_{2h} for the optimized minimum energy structures (except where noted in the Supplementary Information). The vertical electronic transitions of gas-phase structure-optimized triiodide and tetraiodide (both are linear) in the UV-Vis region were calculated using time-dependent DFT (TDDFT). For comparison, TDDFT calculations were also performed for "straight" and "bent" triiodides obtained from CASTEP optimization mentioned before to explore the effects of bond lengths and angles on the electronic structure. In the "straight" triiodide, ∠(I-I-I) = 177.6° and the bond lengths are 2.928 Å and 2.867 Å; In the "bent" triiodide, ∠(I-I-I) = 173.8° and the bond lengths are 2.950 Å and 2.910 Å. Calculations for these two structures were performed in C_s symmetry (Supplementary Table 5-6). Both DFT and TDDFT calculations in gas phase and in PCMs were performed with the SDB-aug-cc-pVTZ basis set[50] using Gaussian 09 Revision A.02. The unrestricted formalism was employed to describe the doublet spin multiplicity of ground-state diiodide and tetraiodide.

Data availability. The datasets generated and/or analyzed during the current study are available from the corresponding author on reasonable request.

References

1. Nitzan, A. *Chemical Dynamics in Condensed Phases: Relaxation, Transfer and Reactions in Condensed Molecular Systems*. (Oxford University Press, 2006).
2. Harris, A. L., Brown, J. K. & Harris, C. B. The nature of simple photodissociation reactions in liquids on ultrafast time scales. *Annu. Rev. Phys. Chem.* **39,** 341–366 (1988).
3. Owrutsky, J. C., Raftery, D. & Hochstrasser, R. M. Vibrational relaxation dynamics in solutions. *Annu. Rev. Phys. Chem.* **45,** 519–55 (1994).
4. Elles, C. G. & Crim, F. F. Connecting chemical dynamics in gases and liquids. *Annu. Rev. Phys. Chem.* **57,** 273–302 (2006).
5. Carpenter, B. K., Harvey, J. N. & Orr-Ewing, A. J. The Study of Reactive Intermediates in Condensed Phases. *J. Am. Chem. Soc.* **138,** 4695–705 (2016).
6. Apkarian, V. A. & Schwentner, N. Molecular Photodynamics in Rare Gas Solids. *Chem. Rev.* **99,** 1481–1514 (1999).
7. Hoops, A. A., Gascooke, J. R., Faulhaber, A. E., Kautzman, K. E. & Neumark, D. M. Two- and three-body photodissociation of gas phase I(3) (-). *J. Chem. Phys.* **120,** 7901–9 (2004).
8. Nakanishi, R. *et al.* Photodissociation of gas-phase I3-: comprehensive understanding of nonadiabatic dissociation dynamics. *J. Chem. Phys.* **126,** 204311 (2007).
9. Banin, U. & Ruhman, S. Ultrafast photodissociation of I3. Coherent photochemistry in solution. *J. Chem. Phys.* **98,** 4391 (1993).
10. Kühne, T. & Vöhringer, P. Vibrational relaxation and geminate recombination in the femtosecond-photodissociation of triiodide in solution. *J. Chem. Phys.* **105,** 10788 (1996).
11. Poulin, P. R. Coherent lattice and molecular dynamics in ultrafast single-shot spectroscopy. (Massachusetts Institute of Technology, 2005).
12. Nishiyama, Y., Terazima, M. & Kimura, Y. Ultrafast relaxation and reaction of diiodide anion after photodissociation of triiodide in room-temperature ionic liquids. *J. Phys. Chem. B* **116,** 9023–32 (2012).
13. Poulin, P. R. & Nelson, K. A. Irreversible Organic Crystalline Chemistry Monitored in Real Time. *Science* **313,** 1756–1760 (2006).
14. Gershgoren, E., Banin, U. & Ruhman, S. Caging and Geminate Recombination following Photolysis of Triiodide in Solution. *J. Phys. Chem. A* **102,** 9–16 (1998).
15. Johnson, A. E. & Myers, A. B. Solvent Effects in the Raman Spectra of the Triiodide Ion: Observation of Dynamic Symmetry Breaking and Solvent Degrees of Freedom. *J. Phys. Chem.* **100,** 7778–7788 (1996).
16. Kim, K. H. *et al.* Solvent-Dependent Molecular Structure of Ionic Species Directly Measured by Ultrafast X-Ray Solution Scattering. *Phys. Rev. Lett.* **110,** 165505 (2013).
17. Svensson, P. H. & Kloo, L. Synthesis, structure, and bonding in polyiodide and metal iodide-iodine systems. *Chem. Rev.* **103,** 1649–84 (2003).
18. Gabes, W. & Gerding, H. Vibrational spectra and structures of the trihalide ions. *J. Mol. Struct.* **14,** 267–279 (1972).
19. Zambounis, J. S., Kamitsos, E. I., Patsis, A. P. & Papavassiliou, G. C. Resonance Raman and far-infrared studies of n-Bu4NI3 and n-Bu4NBr3. *J. Raman Spectrosc.* **23,** 81–85 (1992).
20. Broude, V. L., Rashba, E. I. & Sheka, E. F. *Spectroscopy of Molecular Excitons*. (Springer, 1985).
21. Brotherton, W. S., Clark, R. J. & Zhu, L. Synthesis of 5-iodo-1,4-disubstituted-1,2,3-triazoles mediated by in situ generated copper(I) catalyst and electrophilic triiodide ion. *J. Org. Chem.* **77,** 6443–55 (2012).
22. Kühne, T., Küster, R. & Vöhringer, P. Femtosecond photodissociation of triiodide in solution: Excitation energy dependence and transition state

dynamics. *Chem. Phys.* **233,** 161–178 (1998).

23. Fornier de Violet, P., Bonneau, R. & Joussot-Dubien, J. Laser flash photolysis of iodine-iodide mixture in hydroxylic solvent. Evidence for the existence of the radical anion I4-. *Chem. Phys. Lett.* **28,** 569–572 (1974).
24. Baratz, A. & Ruhman, S. UV photolysis of I3- in solution – Multiple product channels detected by transient hyperspectral probing. *Chem. Phys. Lett.* **461,** 211–217 (2008).
25. Prokhorenko, V. I. Global analysis of multi-dimensional experimental data. *Eur. Photochem. Assoc. Newsl.* 21 (2012).
26. Stoica, P. & Moses, R. L. *Spectral Analysis of Signals*. (Pearson Prentice Hall, 2005).
27. Mallat, S. *A Wavelet Tour of Signal Processing: The Sparse Way*. (Academic Press, 2008).
28. Brazard, J., Bizimana, L. A., Gellen, T., Carbery, W. P. & Turner, D. B. Experimental Detection of Branching at a Conical Intersection in a Highly Fluorescent Molecule. *J. Phys. Chem. Lett.* **7,** 14–9 (2016).
29. Pollard, W. T. *et al.* Theory of dynamic absorption spectroscopy of nonstationary states. 4. Application to 12-fs resonant impulsive Raman spectroscopy of bacteriorhodopsin. *J. Phys. Chem.* **96,** 6147–6158 (1992).
30. Wang, Q., Schoenlein, R., Peteanu, L., Mathies, R. & Shank, C. Vibrationally coherent photochemistry in the femtosecond primary event of vision. *Science* **266,** 422–424 (1994).
31. de Violet, P. F. Polyhalide radical anions as intermediates in chemistry. *Rev. Chem. Intermed.* **4,** 121–169 (1981).
32. Shida, T., Takahashi, Y., Hatano, H. & Imamura, M. Electronic structures of I2− and I4− ions in γ-irradiated rigid solutions. *Chem. Phys. Lett.* **33,** 491–494 (1975).
33. Johnson, P. J. M. *et al.* Local vibrational coherences drive the primary photochemistry of vision. *Nat. Chem.* **7,** 980–986 (2015).
34. Müller, M. *et al.* Anion-π interactions in salts with polyhalide anions: trapping of I4(2-). *Chemistry* **16,** 12446–53 (2010).
35. Manca, G., Ienco, A. & Mealli, C. Factors Controlling Asymmetrization of the Simplest Linear I 3 – and I 4 2– Polyiodides with Implications for the Nature of Halogen Bonding. *Cryst. Growth Des.* **12,** 1762–1771 (2012).
36. Tellinghuisen, J. Analysis of the visible absorption spectrum of I2 in inert solvents using a physical model. *J. Phys. Chem. A* **116,** 391–8 (2012).
37. Groenewald, F., Esterhuysen, C. & Dillen, J. Extensive theoretical investigation: Influence of the electrostatic environment on the I3-...I3- anion-anion interaction. *Theor. Chem. Acc.* **131,** 1–12 (2012).
38. Guo, Z., Molesky, B. P., Cheshire, T. P. & Moran, A. M. Elucidation of reactive wavepackets by two-dimensional resonance Raman spectroscopy. *J. Chem. Phys.* **143,** 124202 (2015).
39. Schwartz, B. J., King, J. C. & Harris, C. B. in *Ultrafast Dynamics of Chemical Systems* 235–248 (Springer Netherlands, 1994).
40. Mukamel, S. *Principles of Nonlinear Optical Spectroscopy*. (Oxford University Press, 1999).
41. Orr-Ewing, A. J. Perspective: Bimolecular chemical reaction dynamics in liquids. *J. Chem. Phys.* **140,** 90901 (2014).
42. Sherwood, P. M. A. *Vibrational spectroscopy of solids*. (Cambridge University Press, 1972).
43. Marino, A. *et al.* Activation of coherent lattice phonon following ultrafast molecular spin-state photo-switching: A molecule-to-lattice energy transfer. *Struct. Dyn. (Melville, N.Y.)* **3,** 23605 (2016).
44. Field, R., Liu, L. C., Gawelda, W., Lu, C. & Miller, R. J. D. Spectral Signatures of Ultrafast Spin Crossover in Single Crystal [Fe(II) (bpy)3](PF6)2. *Chemistry* **22,** 5118–22 (2016).
45. Gühr, M. in *Coherent Vibrational Dynamics* (CRC Press, 2007).
46. Miller, R. J. D. Femtosecond crystallography with ultrabright electrons and x-rays: capturing chemistry in action. *Science* **343,** 1108–16 (2014).

47. Kirchner, F. O., Lahme, S., Riedle, E. & Baum, P. All-reflective UV-VIS-NIR transmission and fluorescence spectrometer for µm-sized samples. *AIP Adv.* **4,** 77134 (2014).

48. Perdew, J. P., Burke, K. & Ernzerhof, M. Generalized Gradient Approximation Made Simple. *Phys. Rev. Lett.* **77,** 3865–3868 (1996).

49. Tkatchenko, A. & Scheffler, M. Accurate Molecular Van Der Waals Interactions from Ground-State Electron Density and Free-Atom Reference Data. *Phys. Rev. Lett.* **102,** 73005 (2009).

50. Martin, J. M. L. & Sundermann, A. Correlation consistent valence basis sets for use with the Stuttgart–Dresden–Bonn relativistic effective core potentials: The atoms Ga–Kr and In–Xe. *J. Chem. Phys.* **114,** 3408 (2001).

Acknowledgement

We thank Arend G. Dijkstra and Michal A. Kochman for helpful discussions, and Daniel S. Badali for contributions to the initial development of the transient absorption setup. This work was funded by the Max Planck Society with additional support from the Hamburg Centre for Ultrafast Imaging. G.C. acknowledges the support from the Alexander von Humboldt Foundation. D.M.R. and C.A.M. acknowledge the UK Car-Parrinello Consortium for allocation of computing time on the EPSRC high performance computing resource ARCHER (managed by the Edinburgh Parallel Computing Centre), the EaStCHEM Research Computing Facility and the University of Edinburgh ECDF facility.

Author contributions

R.J.D.M. conceived the experiment. R.X. grew TBAT crystals and prepared samples for optical measurements. G.C. constructed and programmed the experimental setups and R.X. modified the setups for the current experiment. R.X. performed the measurements with contributions from G.C.. R.X. analyzed and interpreted the data under the supervision of V.I.P and S.A.H.. D.M.R. and C.A.M. carried out the quantum chemical calculations and wrote the theory sections of the manuscript. R.X. wrote the manuscript with contributions from G.C. and V.I.P.. All authors contributed to editing the manuscript to its final form.

Competing financial interests

The authors declare no competing financial interests.

Corresponding author

Correspondence to: R. J. Dwayne Miller.

Figure captions

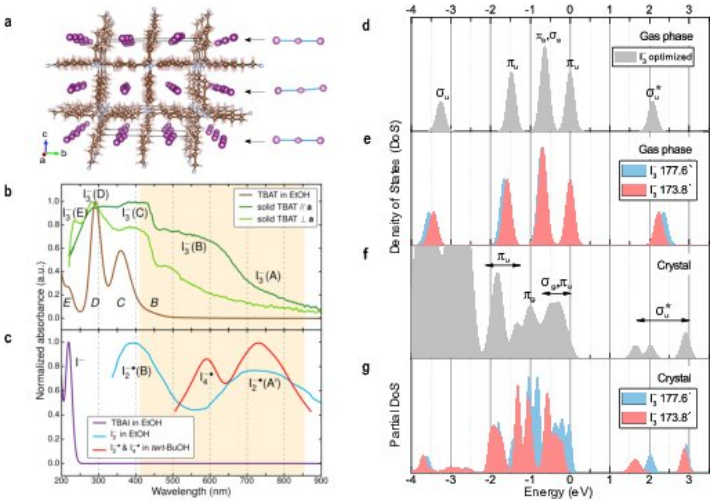

Figure 1. | Crystal and electronic structures of I_3^-. a, Crystal structure[21] of TBAT viewed close to the crystallographic **a** axis. The two types of I_3^- chains ("straight" and "bent") with slightly different opening angles, ∠(I-I-I), are stacked alternately along the **c** axis as indicated by the arrows. The black parallelepiped circumscribes the volume of a unit cell. **b**, Normalized absorption spectra of TBAT in ethanol (EtOH) solution and in solid state. The two solid-state spectra were measured with ultramicrotomed samples and incident broadband light polarized parallel and perpendicular to the **a** axis, respectively. **c**, Normalized absorption spectra of the photoproduct $I_2^{-\bullet}$ (blue, adapted from Ref. 22) and I^- (purple) in EtOH solution. The red curve represents the absorption profile of coexisting $I_2^{-\bullet}$ and tetraiodide radical anion ($I_4^{-\bullet}$) in tertiary butanol (*tert*-BuOH)[23]. In **b** and **c**, the established spectroscopic nomenclatures are placed next to the corresponding bands or in brackets next to the species' names. The orange-shaded rectangular region in **b**-**c** represents the spectrum of the supercontinuum probe (410-855 nm) in TA experiments. **d**, Density of states (DoS) of the isolated, geometry-optimized I_3^-. **e**, DoS of the isolated, bent (173.8°) and straight (177.6°) I_3^- with geometries from optimization of a deposited TBAT crystal structure[21] (see Supplementary Table 12). **f**, DoS of the TBAT unit cell. **g**, Partial DoS of the I_3^- cations, including, respectively, the straight and bent chains. The HOMO energies in gas-phase calculations and the Fermi energies in solid-state calculations are aligned to the energy axis origin for better comparison. The MO labels in **e** follow those in **d**, while those in **g** follow **f**.

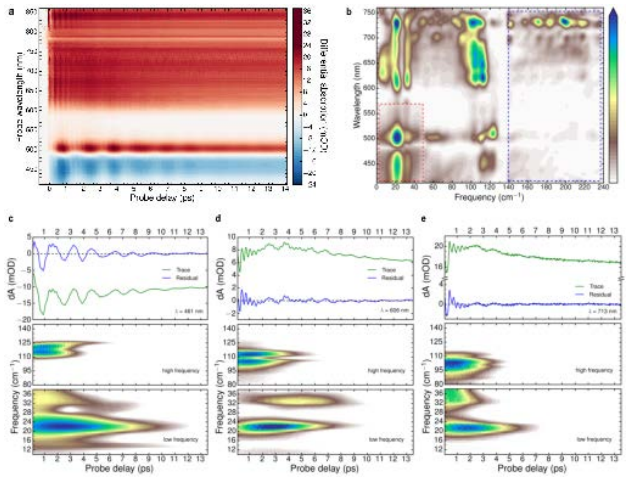

Figure 2. | Short-time dynamics and frequency analysis. a, Differential absorption (dA) of TBAT measured up to a probe delay of ~ 14 ps after photoexcitation. **b**, The 2D power spectrum (up to 240 cm^{-1}) across the probe wavelengths of 412-760 nm calculated with Welch's frequency estimation method[26]. The frequency contents include libration, bending and stretching vibrations, the combination modes, etc (see Supplementary Table 1). **c**-**e**, Time-frequency analysis. In each panel, the TA trace and its residual from removal of the population dynamics are followed by wavelet spectrograms in two frequency ranges, showing the temporal evolution of the major molecular and lattice modes of the relevant chemical species. The data starting from ~ 100 fs after time zero were used for analysis. The low frequency range features the libration modes (22 cm^{-1}, 31 cm^{-1} for $\mathbf{I_3^-}$ in TBAT); the high frequency range features the stretching modes of polyiodides (i.e. $\mathbf{I_n^-}$, where n=2, 3, 4, …). The delayed appearance of the 33 cm^{-1} mode is in accordance with a growing signature in the corresponding TA trace, whereas the onset of the stretching modes are more aligned to the time zero, implying impulsive excitation. For better presentation of the fine details, gamma correction (see Supplementary Information, Section 2) was used to rescale the regions in **b** marked by dashed rectangles (red scaled down and blue scaled up) and the low frequency panel in **c**.

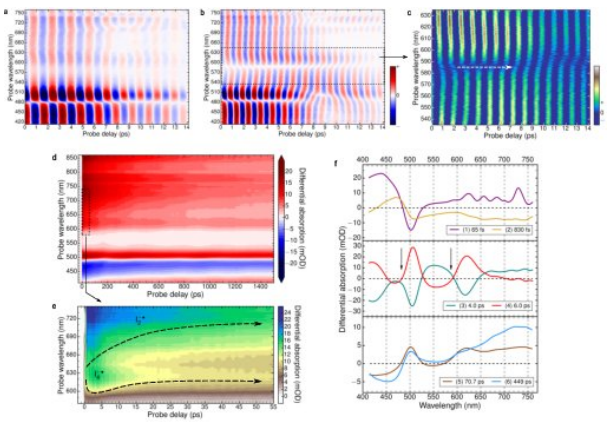

Figure 3. | Evidence of $I_4^{-\bullet}$ formation. The TA residuals Fourier-filtered at 22 cm^{-1} and 33 cm^{-1} are shown in **a** and **b**, respectively. These results show π phase jumps across the nodes at 482 nm (both 22 cm^{-1} and 33 cm^{-1} modes) and 587 nm (only 33 cm^{-1} mode). **c**, Zoomed-in plot of the dashed region around in **b**. In this color scheme, the delayed appearance of the π phase jump across the 587 nm node (marked by the white dashed arrow) and the change of the amplitude of the oscillations on the short and long wavelength sides of the node become more visible. **d,** TA spectra measured with unequally distributed time steps at a probe delay up to 1.5 ns after photoexcitation. **e**, Zoomed-in plot of the dashed region in **d** with a more discerning color scheme to reveal the delayed onset of the TA band associated with $I_4^{-\bullet}$, in respect of $I_2^{-\bullet}$, as traced out by the dashed arrows. **f**, Decay associated spectra (DAS) in the spectral region of 412-760 nm obtained from global analysis of the data of Fig. 2a and **d**. The arrows indicate the wavelength regions of the nodes shown in **a**-**b**.

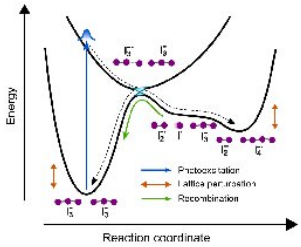

Figure 4. | Possible reaction mechanism of I_3^- in solid-state TBAT. C-band photoexcitation of I_3^- (to the excited state I_3^{-*}) triggers a dissociation reaction. The excited I_3^{-*} crosses at least one conical intersection[8] to form $I_2^{-\bullet}$ in its electronic ground state and $I^\bullet$ with a reasonable amount of translation energy. According to the crystal structure, $I^\bullet$ then needs to travel < 1 Å along the direction of the intermolecular vector between neighboring I_3^- chains before forming a bond with an adjacent I_3^- upon reactive encounter to yield $I_4^{-\bullet}$. The resulting diiodide-tetraiodide configuration ($I_2^{-\bullet} \cdots I_4^{-\bullet}$) likely sits in an energy local minimum nearby the global minimum of the triiodide dimer configuration ($I_3^- \cdots I_3^-$) along the reaction coordinate. The attractive nature of the intermolecular potential at long separation distance indicates that the three-species intermediate (i.e. $I_2^{-\bullet}$, $I^\bullet$ and I_3^-) will have an overall higher system energy than the $I_2^{-\bullet} \cdots I_4^{-\bullet}$ configuration. Since the electrostatic environment can stabilize the $I_3^- \cdots I_3^-$ configuration in the solid state by providing attractive interaction to overcome the Coulomb repulsion between these ions[37], over time, $I_2^{-\bullet} \cdots I_4^{-\bullet}$ reforms $I_3^- \cdots I_3^-$ through various (e.g. geminate or non-geminate) recombination processes influenced by local lattice perturbations, thereby reversing the reaction.